Screened Coulomb interaction of localized electrons in solids from first principles

Bi-Ching Shih, Yubo Zhang, Wenqing Zhang, and Peihong Zhang

Phys. Rev. B **85**, 045132 — Published 30 January 2012

DOI: 10.1103/PhysRevB.85.045132

Screened Coulomb Interaction of Localized Electrons in Solids from First-Principles

Bi-Ching Shih,[1] Yubo Zhang,[2,3] Wenqing Zhang,[2] and Peihong Zhang[1]

[1]*Department of Physics,University at Buffalo, State University of New York, Buffalo, New York 14260, USA*
[2]*State Key Laboratory of High Performance Ceramics and Superfine Microstructures, Shanghai Institute of Ceramics, Chinese Academy of Sciences, Shanghai 200050, China*
[3]*Department of Physics, Harbin Institute of Technology, Harbin 150001, China*

(Dated: January 17, 2012)

We report the implementation of a first-principles approach for calculating the screened Coulomb and exchange energies for localized electrons in solids. Our method is based on the pseudopotential plane wave formalism. The localized orbitals are represented by maximally localized Wannier functions (MLWF), and the screening effects are calculated within the constrained random phase approximation (cRPA). As first applications of this new development, we investigate the on-site Coulomb U and exchange J for the $3d$ electrons in ZnO, NiO, and $CuGaS_2$. Both the bare (unscreened) and the screened U and J matrices are presented. We find that it is very important for these parameters to be calculated self-consistently. Intra-channel (i.e., d-d) and energy-dependent screening effects are also discussed.

PACS numbers: 71.15.Mb,71.28.+d,71.20.Nr,71.10.Fd

I. INTRODUCTION

An accurate account of the screened Coulomb interaction for localized electrons (e.g., d or f electrons) in solids is very important for understanding the structural, electronic, and optical properties of strongly correlated materials. Density functional theory (DFT)[1] based electronic structure methods within the local density approximation (LDA)[2] or the generalized gradient approximation (GGA)[3] have been rather successful in predicting properties of weakly to moderately correlated materials. However, it is well recognized that the LDA (or GGA) fails in many aspects when applied to strongly correlated materials such as transition metal oxides due to the insufficient treatment of the correlation effect of localized d and/or f electrons. Several schemes have been proposed to incorporate the strong correlation effects of localized electrons in electronic structure calculations, among them the LDA+U approach[4,5] has been widely adopted because of its clear physical motivation, relatively simple implementation, and low computational cost.

Although the LDA+U method has been applied to the study of transition metal oxides with significant successes, one major uncertainty is the use of adjustable parameters, i.e., the on-site screened Coulomb energy U (also known as the Hubbard U) and the exchange energy J for localized electrons. This seriously compromises the predictive power of the LDA+U method. Moreover, accurate knowledge of the Hubbard U for localized electrons is important not only for electronic structure methods such as the LDA+U method but also for constructing material-specific, effective Hamiltonians that map correlated electron systems to some low energy models for subsequent many-body treatments. Therefore, there is an urgent need that this important parameter be calculated from first-principles.

Several first-principles approaches have been proposed to calculate the U and J parameters for correlated materials containing localized d or f electrons. These methods can be broadly classified into two categories, the constrained LDA (cLDA)[6–8] and the cRPA[9–13] approaches. Regardless of the details of the numerical implementation, there are two essential issues that need to be addressed: a) the definition (or construction) of localized orbitals for which the Hubbard U is to be calculated, and b) the treatment of the screening (renormalization) effects. Atomic-like orbitals used in electronic structure methods such as the linear muffin-tin orbital (LMTO)[14] method may serve as a natural choice for defining localized orbitals. Alternatively, one may use the MLWF[15–17] associated with the localized electrons. The MLWF are the solid-state equivalence of molecular orbitals which often reveal the nature of chemical bonding in solids. This approach also has greater flexibility and can be generalized to describe localized states (e.g., localized defect states) that are not centered at atomic sites. The renormalization effects can then be treated using the cLDA or the cRPA approach.

The essential idea behind the cRPA approach is the removal of the intra-channel (e.g., d-d) electron polarizability from the full polarizability calculated within the random phase approximation (RPA). Aryasetiawan *et al.* have discussed in great details the difference between these two approaches (i.e., cLDA and cRPA) and the advantages of the cRPA approach.[12,13] For example, the cRPA approach allows the evaluation of the full Hubbard U and exchange J matrices and their energy dependence. Inter-site interaction can be calculated easily within the cRPA approach, especially when the MLWF are used, without the need of using large unit cells. The cRPA approach has been implemented predominantly in electronic structure methods that are based on localized orbitals. In this paper, we report a new implementation of the combined MLWF and the cRPA approach within the pseudopotential plane wave formalism and demonstrate its applications to a broad range of systems.

II. METHOD

In solids, the strength of the Coulomb interaction between two electrons is significantly reduced (screened). The screened Coulomb interaction W is related to the bare Coulomb interaction v as $W = \epsilon^{-1}v$, where ϵ^{-1} is the inverse dielectric function. Within the RPA, the dielectric function ϵ is related to the electron *irreducible polarizability* P by $\epsilon = 1 - vP$. For periodic solids, it is convenient to express the polarizability and dielectric function in the plane wave basis:

$$P_{\mathbf{GG}'}(\mathbf{q},\omega) = \sum_{\mathbf{k},n,n'} \langle n\mathbf{k}|e^{-i(\mathbf{q}+\mathbf{G})\cdot\mathbf{r}}|n'\mathbf{k}+\mathbf{q}\rangle \cdot \langle n'\mathbf{k}+\mathbf{q}|e^{i(\mathbf{q}+\mathbf{G}')\cdot\mathbf{r}'}|n\mathbf{k}\rangle \frac{f_{n'\mathbf{k}+\mathbf{q}} - f_{n\mathbf{k}}}{\epsilon_{n'\mathbf{k}+\mathbf{q}} - \epsilon_{n\mathbf{k}} + \omega + i\delta}, \quad (1)$$

and

$$\epsilon_{\mathbf{GG}'}(\mathbf{q},\omega) = \delta_{\mathbf{GG}'} - v(\mathbf{q}+\mathbf{G})P_{\mathbf{GG}'}(\mathbf{q},\omega). \quad (2)$$

In the above equations, $|n\mathbf{k}\rangle$ are the Kohn-Sham eigenstates, $\epsilon_{n\mathbf{k}}$ and $f_{n\mathbf{k}}$ are the corresponding eigenvalues and electron occupation numbers, and $v(\mathbf{q}+\mathbf{G})$ is the Fourier transform of the bare Coulomb potential. The screened Coulomb potential is then

$$W_{\mathbf{GG}'}(\mathbf{q},\omega) = \frac{4\pi}{\Omega}\epsilon^{-1}_{\mathbf{GG}'}(\mathbf{q},\omega)\frac{1}{|\mathbf{q}+\mathbf{G}'|^2}, \quad (3)$$

where Ω is the crystal volume.

With properly constructed localized orbitals, the screened Coulomb and exchange energies can be evaluated:

$$U_{ij} = \langle ij|W|ij\rangle = \int d\mathbf{r}d\mathbf{r}'|\phi_i(\mathbf{r})|^2 W(\mathbf{r},\mathbf{r}')|\phi_j(\mathbf{r}')|^2, \quad (4)$$

and

$$J_{ij} = \langle ij|W|ji\rangle = \int d\mathbf{r}d\mathbf{r}'\phi^*_i(\mathbf{r})\phi^*_j(\mathbf{r}')W(\mathbf{r},\mathbf{r}')\phi_i(\mathbf{r}')\phi_j(\mathbf{r}), \quad (5)$$

where ϕ_i and ϕ_j are the localized orbitals of interest.

In this work, the localized orbitals are constructed using the MLWF method[15,16] as implemented in the WANNIER90 package.[17] The MLWF are constructed by performing a unitary transformation of relevant Bloch states:

$$\begin{aligned}\phi_{n\mathbf{R}}(\mathbf{r}) &= \frac{1}{\sqrt{N_k}}\sum_{\mathbf{k},m}\mathbb{U}^{(\mathbf{k})}_{nm}\psi_{m\mathbf{k}}(\mathbf{r})e^{i\mathbf{k}\cdot\mathbf{R}} \\ &= \frac{1}{\sqrt{N_k}}\sum_{\mathbf{k}}\tilde{\psi}_{n\mathbf{k}}e^{i\mathbf{k}\cdot\mathbf{R}} \\ &= \frac{1}{\sqrt{N_k}}\sum_{\mathbf{k}}\tilde{u}_{n\mathbf{k}}e^{i\mathbf{k}\cdot(\mathbf{r}+\mathbf{R})}, \end{aligned} \quad (6)$$

where $\phi_{n\mathbf{R}}$ are the MLWF centralized at cell $\mathbf{R}$, N_k is the number of k-points used in the Brillouin zone summation, $\psi_{m\mathbf{k}}$ are the Bloch wave functions, $\tilde{\psi}_{n\mathbf{k}}$ are unitarily rotated Bloch wave functions, and $\tilde{u}_{n\mathbf{k}}$ are the periodic part of $\tilde{\psi}_{n\mathbf{k}}$. Within the plane wave basis, the matrix elements U_{ij} and J_{ij} for a given pair of MLWF ϕ_i and ϕ_j can be evaluated in the momentum space:

$$U_{ij} = \sum_{\mathbf{q},\mathbf{G},\mathbf{G}'} F^*_{ii}(\mathbf{G},\mathbf{q})\cdot W_{\mathbf{GG}'}(\mathbf{q})\cdot F_{jj}(\mathbf{G}',\mathbf{q}), \quad (7)$$

and

$$J_{ij} = \sum_{\mathbf{q},\mathbf{G},\mathbf{G}'} F^*_{ij}(\mathbf{G},\mathbf{q})\cdot W_{\mathbf{GG}'}(\mathbf{q})\cdot F_{ji}(\mathbf{G}',\mathbf{q}), \quad (8)$$

where we have defined auxiliary functions F_{ij} as follows:

$$\begin{aligned} F_{ij}(\mathbf{G},\mathbf{q}) &= \int d\mathbf{r}\phi^*_i(\mathbf{r})e^{-i(\mathbf{q}+\mathbf{G})\cdot\mathbf{r}}\phi_j(\mathbf{r}) \\ &= \frac{1}{N_k}\sum_{\mathbf{k}}\int d\mathbf{r}\tilde{u}^*_{i\mathbf{k}}(\mathbf{r})\tilde{u}_{j\mathbf{k}+\mathbf{q}}(\mathbf{r})e^{-i\mathbf{G}\cdot\mathbf{r}}, \end{aligned} \quad (9)$$

which can be evaluated efficiently using the fast Fourier transform technique. In evaluating Eq. (7) and Eq. (8), additional care must be taken to handle the divergence of the Coulomb potential as $\mathbf{q}+\mathbf{G}' \to 0$.[18]

In the approach described above, the dielectric function is calculated within the conventional RPA. It has been pointed out that while constructing an effective Hamiltonian for localized d (or f) electrons, the intra-channel d-d (or f-f) screening effects shall be excluded.[10,11] This is because these d-d screenings are an inherent part of the physics of the subsystem, and they will naturally come into play in the subsequent treatment of the subsystem Hamiltonian. Therefore, the effective Coulomb interaction between localized electrons shall be normalized (screened) only by the rest of the system. Defining a partial (or constrained) polarizability P_c,

$$P_c = P - P_d, \quad (10)$$

where P_d is the polarizability arising from virtual transitions between localized d states (i.e., intra-channel polarizability), the effective Coulomb interaction W_c for the subsystem that does not include the intra-channel screening effects becomes $W_c = (1 - vP_c)^{-1}v$. The screened Coulomb and exchange matrix elements for localized electrons are

$$U_{ij} = \langle ij|W_c|ij\rangle \text{ and } J_{ij} = \langle ij|W_c|ji\rangle. \quad (11)$$

Although the theoretical framework of the cRPA method is physically motivated and well defined, several issues arise when it comes to practical implementations of the method.[13] One major issue is the calculation (or elimination) of the intra-channel polarizability P_d. Except for a few extreme cases, most correlated materials involve entangled states of localized and delocalized (e.g., d and sp) electrons, and the separation of the intra-channel polarizability is not straightforward.[11,13,19] In this work,

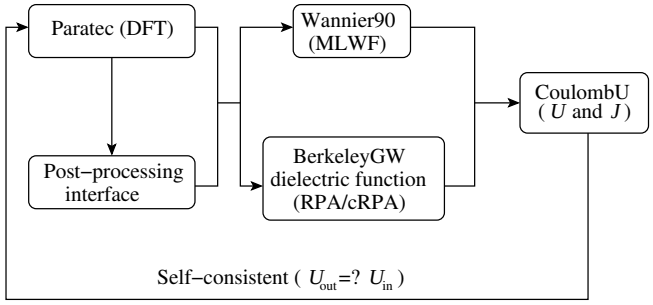

FIG. 1: The structure and computational components of the newly developed package for calculating screened Coulomb U and exchange J using a combined MLWF and cRPA approach.

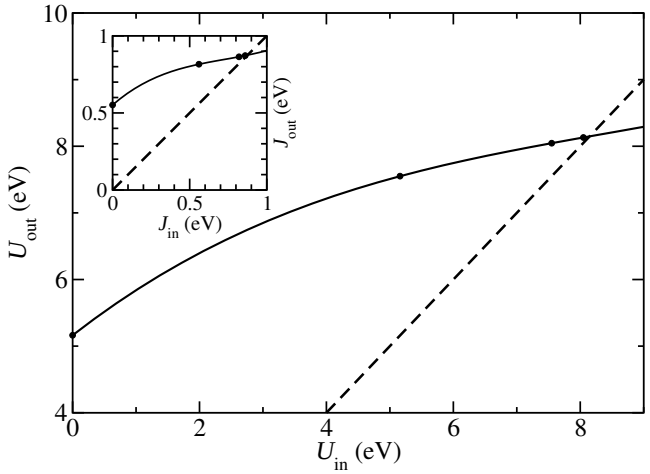

FIG. 2: Convergence behavior of the calculated U and J parameters for the semicore d electrons in zb-ZnO. The self-consistency is reached when $U_{\rm out} = U_{\rm in}$ and $J_{\rm out} = J_{\rm in}$.

we use a wave function projection technique to calculate the intra-channel polarizability:

$$P_d = \sum_{\mathbf{k},n,n',i,j} |C^i_{n\mathbf{k}}|^2 |C^j_{n'\mathbf{k}+\mathbf{q}}|^2 \langle n\mathbf{k}|e^{-i(\mathbf{q}+\mathbf{G})\cdot\mathbf{r}}|n'\mathbf{k}+\mathbf{q}\rangle \cdot \langle n'\mathbf{k}+\mathbf{q}|e^{i(\mathbf{q}+\mathbf{G}')\cdot\mathbf{r}'}|n\mathbf{k}\rangle \cdot \frac{f_{n'\mathbf{k}+\mathbf{q}} - f_{n\mathbf{k}}}{\epsilon_{n'\mathbf{k}+\mathbf{q}} - \epsilon_{n\mathbf{k}} + \omega + i\delta}, \quad (12)$$

where $C^i_{n\mathbf{k}} = \langle \phi_{d_i}|n\mathbf{k}\rangle$ is the projection of a Bloch wave function $|n\mathbf{k}\rangle$ onto a localized orbital ϕ_{d_i}.

III. COMPUTATIONAL DETAILS

The program structure and the calculation procedure of our computational package is shown in Fig. 1. First, DFT calculations within the LDA (or GGA) or LDA+U are carried out using the PARATEC package.[20,21] A post-processing interface is developed to generate necessary output for subsequent calculations. We use the WANNIER90 package[17] to construct the MLWF and the BerkeleyGW package[22] to calculate the dielectric function within the RPA or cRPA. In the last step, the CoulombU program calculates the screened Coulomb and exchange matrix elements. The familiar U and J parameters used in the LDA+U calculations are the average values of the full Coulomb and exchange matrices:

$$U = \frac{1}{(2l+1)^2}\sum_{ij} U_{ij} \text{ and } J = \frac{1}{2l(2l+1)}\sum_{i\neq j} J_{ij}, \quad (13)$$

where $l = 2$ for d electrons.

It is sometimes desirable to calculate the U and J parameters self-consistently. This is particularly important for systems for which the LDA (or GGA) cannot provide a faithful description of the electronic structure. A typical calculation starts with some initial guess for the U and J parameters. The calculation is iterated until a self-consistency is reached. Figure 2 shows the convergence behavior for the calculated U and J for the semicore d electrons in zinc-blende (zb) ZnO. With a reasonable initial guess, a self-consistent result can be achieved within three or four iterations. We mention that a large input U value will lead to slightly more localized Wannier functions. We will discuss this in more details later.

We apply this new implementation to study the screened on-site Coulomb and exchange energies of localized $3d$ electrons in a range of materials, including ZnO, a technological important semiconductor that contains shallow semicore d electrons, NiO, a classic and intensively discussed Mott-Hubbard insulator, and $CuGaS_2$, the parent material for a large class of Cu based semiconductors that are collectively known as CIGS ($CuIn_xGa_{1-x}S_ySe_{2-y}$) which are among the most promising materials for thin film solar cell applications.

We use the Troullier-Martins norm-conserving pseudopotentials,[23] and all semicore subshells (i.e., $3s$, $3p$, and $3d$) of Zn, Cu, and Ni are included in our calculation. The kinetic energy cutoff for the plane wave expansion is 350 Ry for ZnO, 300 Ry for $CuGaS_2$, and 250 Ry for NiO. The k-point sampling is generated using the Monkhorst-Pack scheme[24] with a $6 \times 6 \times 6$ density for zb-ZnO. We also investigate the wurtzite (wz) structure of ZnO. However, the discussions will be mostly focused on zb-ZnO for simplicity. Similar k-point densities are used for other systems. The energy cutoff of 40 Ry is used for truncating the dielectric matrix.

IV. RESULTS

A. ZnO

As a first application of our program, we investigate the screened on-site Coulomb U and exchange J for the semicore d electrons in ZnO. ZnO is a technologically important material that holds great promise for optoelectronics and spintronics applications.[25,26] Surprisingly, although being a "simple" sp semiconductor, ZnO defies

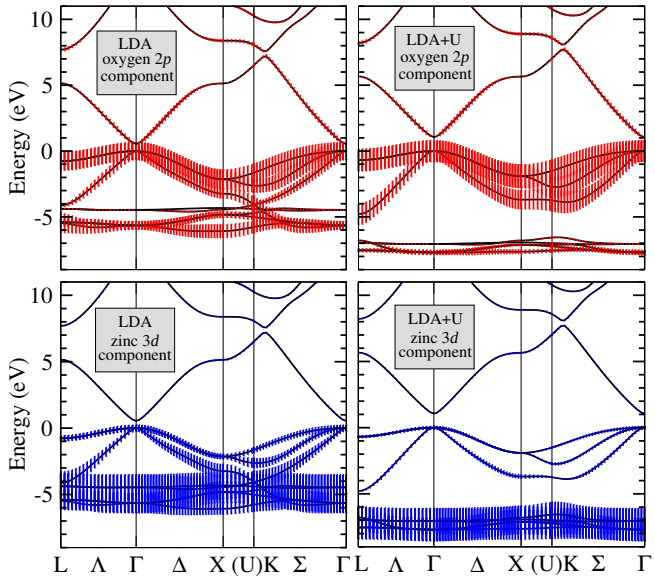

FIG. 3: (Color online) The LDA (left panels) and LDA+U (right panels) band structures of zb-ZnO. Projections of the band wave functions onto O $2p$ (top panels) and Zn $3d$ (bottom panels) orbitals are shown as vertical bars superimposed on the band structures.

several previous attempts to understand its electronic structure. Much of the theoretical difficulty has been attributed to the inadequate treatment of the semicore d states within the LDA or GGA. Since all d states are fully occupied in ZnO, the dielectric function is calculated within the conventional RPA approach without any constraints.

We start our discussions by taking a closer look at the electronic band structure of zb-ZnO calculated within the LDA as shown in the left panels of Fig. 3. The electronic structure of wz-ZnO shows similar characteristics.[27] Superimposed on the band structure are projections (indicated by vertical bars) of band wave functions onto the oxygen $2p$ (left top panel) and the zinc $3d$ (left bottom panel) orbitals. The LDA significantly underestimates the binding energy of d electrons and overestimates the pd hybridization. This enhanced pd hybridization pushes the valence p states up, resulting in a surprisingly small band gap calculated within the LDA. In addition, there is no gap between the d and p bands, and the d derived t_2 triplet entangles with the valence p states. Upon applying an on-site U ($U \sim 8.1$ eV, which is calculated self-consistently as explained in the previous section) in the electronic structure calculation, the d states are fully detached from the valence p states (right panels of Fig. 3), and the width of the d bands is substantially narrower compared with the LDA result. In addition, the pd hybridization is greatly reduced. These differences in electronic structures calculated within the LDA and the LDA+U methods will have significant effects on the construction of MLWF and the calculated U value.

Table I compares the averaged U and J for zb- and wz-ZnO. Both the screened (U^s, J^s) and the bare (U^b, J^b) values are shown. We first calculate the U and J parameters for zb-ZnO using the LDA Kohn-Sham eigen solution. Although the O p- and Zn d-bands calculated within the LDA are entangled (see Fig. 3), it is still possible to construct d-like Wannier functions using a disentanglement technique developed by Souza *et al.*[16] However, due to the strong pd hybridization (which is largely unphysical), one would expect that the Wannier orbitals so constructed might not faithfully represent the d states in this system. In fact, the average on-site U is only 5.2 eV calculated with the LDA solutions, whereas the U value calculated self-consistently with the LDA+U method is about 8.1 eV (8.0 eV wz-ZnO). The bare Coulomb U calculated with the LDA method is 17.8 eV for zb-ZnO (17.4 eV for wz-ZnO), to be compared with 25.3 eV (24.6 eV for wz-ZnO) calculated self-consistently with the LDA+U method. The calculated exchange J shows a similar enhancement us-

TABLE I: Average values of direct Coulomb and exchange energies (in eV) for zinc $3d$-electrons in zb- and wz-ZnO. We show both the bare and the screened values calculated using the LDA and LDA+U methods.

	zb-ZnO		wz-ZnO	
	(U^b, J^b)	(U^s, J^s)	(U^b, J^b)	(U^s, J^s)
LDA	(17.8, 0.61)	(5.2, 0.55)	(17.4, 0.61)	(5.2, 0.54)
LDA+U	(25.3, 0.94)	(8.1, 0.87)	(24.6, 0.91)	(8.0, 0.84)

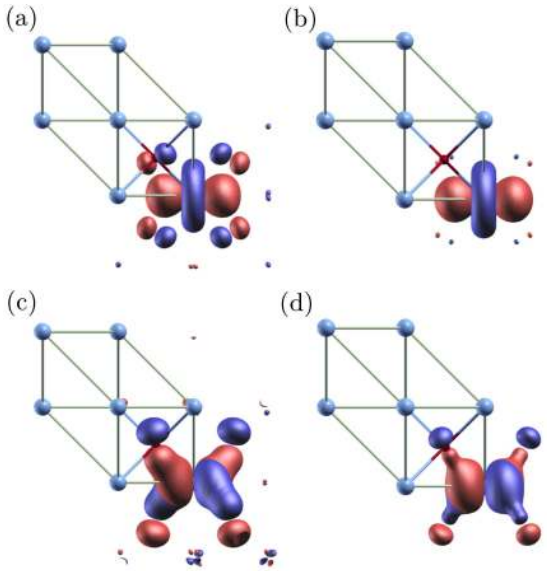

FIG. 4: (Color online) Two representative Zn d-like MLWF optimized using the WANNIER90 package. (a) and (b): d-like MLWF with the e symmetry; (c) and (d): d-like MLWF with the t_2 symmetry. The MLWF on the left are constructed with the LDA solution whereas those on the right are constructed with the LDA+U solution.

TABLE II: Screened (bare values in parentheses) Coulomb and exchange matrix elements for 3d electrons in zb-ZnO. All values are in eV.

	U^s_{ij} (U^b_{ij})					J^s_{ij} (J^b_{ij})				
	$e^{(1)}$	$e^{(2)}$	$t_2^{(1)}$	$t_2^{(2)}$	$t_2^{(3)}$	$e^{(1)}$	$e^{(2)}$	$t_2^{(1)}$	$t_2^{(2)}$	$t_2^{(3)}$
$e^{(1)}$	10.0 (27.9)	7.7 (25.4)	8.2 (25.5)	8.2 (25.5)	7.5 (24.6)		1.12 (1.22)	0.68 (0.71)	0.68 (0.71)	1.08 (1.18)
$e^{(2)}$	7.7 (25.4)	10.0 (27.9)	7.7 (24.9)	7.7 (24.9)	8.5 (25.8)	1.12 (1.22)		0.95 (1.02)	0.95 (1.02)	0.55 (0.56)
$t_2^{(1)}$	8.2 (25.5)	7.7 (24.9)	9.3 (26.1)	7.4 (24.1)	7.4 (24.1)	0.68 (0.71)	0.95 (1.02)		0.91 (0.99)	0.91 (0.99)
$t_2^{(2)}$	8.2 (25.5)	7.7 (24.9)	7.4 (24.1)	9.3 (26.1)	7.4 (24.1)	0.68 (0.71)	0.95 (1.02)	0.91 (0.99)		0.91 (0.99)
$t_2^{(3)}$	7.5 (24.6)	8.5 (25.8)	7.4 (24.1)	7.4 (24.1)	9.3 (26.1)	1.08 (1.18)	0.55 (0.56)	0.91 (0.99)	0.91 (0.99)	
Average			8.1 (25.3)					0.87 (0.94)		

ing the LDA+U method.

The difference in the U values calculated using the LDA and LDA+U methods comes largely from the difference in the localization of Wannier orbitals. The separation between the p and d bands calculated with the LDA+U method results in more localized Wannier orbitals. Figure 4 compares the d-like MLWF constructed using the LDA and the LDA+U solutions. We show only two representative d Wannier orbitals, one with the e symmetry and the other with the t_2 symmetry. The MLWF constructed using the LDA eigenstates (left panels of Fig. 4) show substantial weights on oxygen sites, indicating the involvement of p states in the MLWF. The MLWF constructed with the LDA+U eigenstates (right panels of Fig. 4) are more localized, and the involvement of the oxygen p states is significantly reduced.

Table II shows the full U and J matrices for zb-ZnO calculated self-consistently using the LDA+U method. The bare values (U^b and J^b) are shown in parentheses. The bare Coulomb matrix elements range from 24.1 to 27.9 eV with an averaged value of 25.3 eV. The diagonal elements (27.9 eV and 26.1 eV) are very close to the atomic value of 28.8 eV calculated using the Hartree-Fock approximation.[28] The screened Coulomb energy U^s ranges from 7.4 to 10.0 eV with an averaged value of 8.1 eV. This gives an effective screening $\bar{\epsilon}$ for the on-site Coulomb U of 25.3/8.1 = 3.1 for zb-ZnO. It is interesting to note that the matrix elements for the e doublet are slightly larger than those for the t_2 triplet. This is expected since the d-t_2 states hybridize with oxygen p states, resulting in a slightly larger Wannier spread than that of the MLWF with the e symmetry.

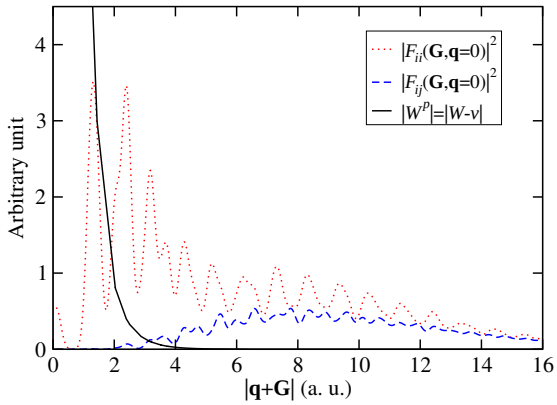

FIG. 5: (Color online) Comparison between the auxiliary functions $F_{ii}(\mathbf{G},\mathbf{q}=0)$ (dotted line) and $F_{ij}(\mathbf{G},\mathbf{q}=0)$ (dashed line) involved in the calculation of U and J parameters. The diagonal part of the polarization potential (solid line) is also plotted to illustrate the effectiveness of the screening effects on the Coulomb U and exchange J.

The bare exchange matrix elements range from 0.56 to 1.22 eV with an average value of 0.94 eV. Interestingly, the averaged screened exchange (J^s = 0.87 eV) is only slightly smaller than the bare value, indicating that the screening effects are less effective for the exchange interaction. Similar observations have been reported.[19,28,29] However, to the best of our knowledge, no detailed explanations have been given so far. The effectiveness of the screening effects on the Coulomb U and exchange J can be understood by taking a closer look at Eqs. (7)−(9). Whereas the calculation of the Coulomb U involves the Fourier transform of the charge density of Wannier functions, i.e., F_{ii} and F_{jj} in Eq. (7), that for the exchange J involves F_{ij} which is the Fourier transform of the product of two different Wannier functions. Figure 5 plots $F_{ii}(\mathbf{G},\mathbf{q}=0)$ and $F_{ij}(\mathbf{G},\mathbf{q}=0)$ together with the diagonal elements of the polarization potential $W^p_{\mathbf{GG}}(\mathbf{q}=0) = (W-v)_{\mathbf{GG}}(\mathbf{q}=0)$. The function $F_{ij}(\mathbf{G},\mathbf{q})$ has appreciable magnitude only at substantially large $\mathbf{G}$ values. The function $F_{ii}(\mathbf{G},\mathbf{q})$, on the other hand, has substantial weights at small $\mathbf{G}$ values. Since the screening is less effective at large $\mathbf{G}$ (the polarization potential is very small at large $\mathbf{G}$), the screening effects on the exchange J are unsubstantial for 3d states.

B. NiO

Late transition metal (TM) monoxides (MnO, FeO, CoO, NiO, and CuO) are prototypical examples of strongly correlated materials and attempts to understand their electronic, magnetic, and optical properties using DFT based first-principles methods have been hindered by the inadequate treatment of the correlation effects among localized d electrons. The on-site Coulomb U is recognized as one of the most important characteristic

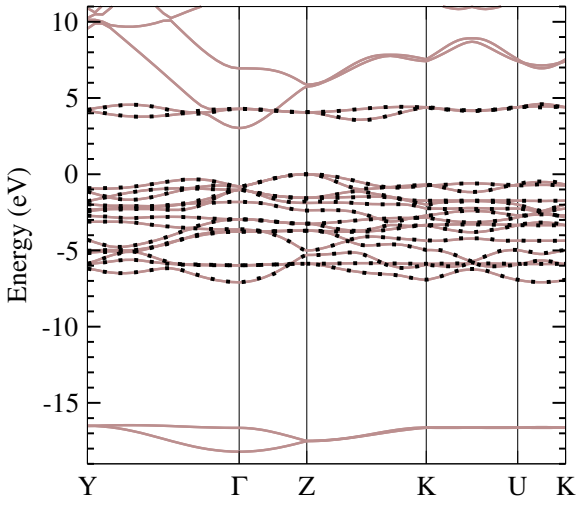

FIG. 6: (Color online) Band structure of antiferromagnetic NiO calculated using the LDA+U method. The black dots are the band structure reconstructed using the MLWF.

energy scales in these systems. Among all TM monoxides, NiO has probably received the most research attention. There have been several previous calculations of Coulomb U for NiO using both first-principles and empirical approaches.[4,8,30–35] Therefore, NiO serves as a very good example for comparing results obtained by different approaches. In addition, since the d states are partially occupied in NiO, there will be substantial intra-channel screening, and it is very important to study the effects of intra-channel screening on the calculated Coulomb U.

Below the Neel temperature, NiO assumes a type-II antiferromagnetic (AFM-II) structure, in which the AFM ordering occurs along the $\langle 111 \rangle$ direction. As a result of the AFM ordering, the otherwise cubic rock-salt lattice is slightly compressed along the $\langle 111 \rangle$ direction. We use the AFM-II phase NiO as an example to demonstrate the calculation of spin-dependent Coulomb U and exchange J. Similar to the spin-independent case, the spin-dependent U and J matrices can be calculated by evaluating the following integrals:

$$U_{i\sigma j\sigma'} = \langle i\sigma j\sigma' | W | i\sigma j\sigma' \rangle \text{ and } J_{i\sigma j\sigma} = \langle i\sigma j\sigma | W | j\sigma i\sigma \rangle, \tag{14}$$

where σ is the spin index. The average values are

$$U = \frac{1}{4(2l+1)^2} \sum_{i\sigma j\sigma'} U_{i\sigma j\sigma'} \text{ and } J = \frac{1}{4l(2l+1)} \sum_{i \neq j,\sigma} J_{i\sigma j\sigma}. \tag{15}$$

Figure 6 shows the band structure of AFM-II NiO calculated using the LDA+U method with U and J calculated self-consistently. Unlike ZnO in which the p and d bands are fully separated, the occupied d states strongly hybridize with oxygen p states in NiO. The unoccupied d (minority spin e) states, on the other hand, are well separated and only slightly entangled with an s like conduction band. In order to construct the MLWF, we use an outer energy window that includes all p and d states and an inner energy window that includes all occupied pd states. The band structure reconstructed using the subspace spanned by the MLWF is shown in Fig. 6 with black dots. Although we can calculate the U and J parameters for both the p-like and d-like orbitals, for simplicity, we only show the result for d orbitals.

Table III shows the spin-resolved bare Coulomb U and exchange J for d orbitals on one Ni site. The majority spin (up-spin) orbitals are slightly more localized than the minority spin (down-spin) ones as suggested by slightly larger U values. However, the difference is not significant. In addition, e_g orbitals have greater U values than those of t_{2g} orbitals, but again, the difference is rather small. The averaged on-site bare Coulomb energy, $U^b = (U^b_{\uparrow\uparrow} + U^b_{\downarrow\downarrow} + 2U^b_{\uparrow\downarrow})/4$, is 24.7 eV and the averaged bare exchange J is 0.96 eV.

Table IV shows the screened U and J matrices calculated using both the RPA and cRPA formalism. Within the RPA, the spin-averaged on-site U^s is about 5.8 eV. Removal of the intra-channel screening enhances the average U^s value by about 0.8 eV. Thus the effective screening for the on-site Coulomb U is $\bar{\epsilon} = U^b/U^s$(cRPA) = 3.7 in NiO. Table V compares our results with some of the previous work. Except for the work by Anisimov and coworkers[4] which gives a fairly large U value of about 8.0 eV, most later calculations using different implementations of the cLDA approach give substantially smaller values, ranging from 4.6 to 5.8 eV. These results (especially the most recent result of 5.8 eV[33]) are close to our result calculated using the conventional RPA approach. Our cRPA results (U^s = 6.6 eV and J^s = 0.86 eV) are nearly identical to the recent work of Karlsson *et al.*[30] (U^s = 6.6 eV and J^s = 0.9 eV) which is also based on the cRPA approach. There are several factors that may affect the calculated U and J values. However, the choice of local orbitals and the treatment of the screening effects are the most important ones. It is likely that the screening effects were underestimated in the work of Anisimov *et al.*[4] Interestingly, the U values determined empirically[34,35] are very close to our result calculated with the cRPA approach.

As mentioned earlier, one of the important advantages of the cRPA over the cLDA approach is that the frequency-dependence of the Coulomb U can be calculated within the cRPA approach. The frequency dependent behavior of the screened Coulomb U of NiO is shown in Fig. 7. The bare Coulomb U (24.7 eV) is also shown for comparison. The first dip of the screened Coulomb interaction at around ω = 5.0 eV is due to strong interband transitions near this energy. At the high frequency limit, the screened value approaches the bare one as expected. As pointed out by Aryasetiawan *et al.*,[11,12] since the energy dependence of the U value is rather strong and non-trivial even at relatively low energies, it might be important to take this into account when one attempts to construct effective low energy models for strongly correlated materials.

TABLE III: Spin-dependent bare Coulomb U and exchange J matrices of NiO. All values are in eV.

	$e_g^{(1)}$	$e_g^{(2)}$	$t_{2g}^{(1)}$	$t_{2g}^{(2)}$	$t_{2g}^{(3)}$	$e_g^{(1)}$	$e_g^{(2)}$	$t_{2g}^{(1)}$	$t_{2g}^{(2)}$	$t_{2g}^{(3)}$
			$U^b_{i\uparrow j\uparrow}$					$J^b_{i\uparrow j\uparrow}$		
$e_g^{(1)}$	27.5	24.9	25.3	25.3	24.4		1.27	0.75	0.75	1.23
$e_g^{(2)}$	24.9	27.5	24.7	24.7	25.4	1.27		1.07	1.07	0.59
$t_{2g}^{(1)}$	25.3	24.7	26.2	24.2	24.2	0.75	1.07		1.03	1.03
$t_{2g}^{(2)}$	25.3	24.7	24.2	26.2	24.2	0.75	1.07	1.03		1.03
$t_{2g}^{(3)}$	24.4	25.7	24.2	24.2	26.2	1.23	0.59	1.03	1.03	
Average			25.1					0.98		
			$U^b_{i\downarrow j\downarrow}$					$J^b_{i\downarrow j\downarrow}$		
$e_g^{(1)}$	25.9	23.5	24.3	24.3	23.4		1.17	0.71	0.71	1.17
$e_g^{(2)}$	23.5	25.9	23.7	23.7	24.6	1.17		1.02	1.02	0.56
$t_{2g}^{(1)}$	24.3	23.7	25.7	23.7	23.7	0.71	1.02		1.01	1.01
$t_{2g}^{(2)}$	24.3	23.7	23.7	25.7	23.7	0.71	1.02	1.01		1.01
$t_{2g}^{(3)}$	23.4	24.6	23.7	23.7	25.7	1.17	0.56	1.01	1.01	
Average			24.2					0.94		
			$U^b_{i\uparrow j\downarrow}$							
$e_g^{(1)}$	26.6	24.2	24.8	24.8	23.9					
$e_g^{(2)}$	24.2	26.6	24.2	24.2	25.1					
$t_{2g}^{(1)}$	24.8	24.2	25.9	23.9	23.9					
$t_{2g}^{(2)}$	24.8	24.2	23.9	25.9	23.9					
$t_{2g}^{(3)}$	23.9	25.1	23.9	23.9	25.9					
Average			24.7							

TABLE IV: Spin-dependent screened Coulomb U and exchange J matrices of NiO calculated within the cRPA (RPA) method. All values are in eV.

	$e_g^{(1)}$	$e_g^{(2)}$	$t_{2g}^{(1)}$	$t_{2g}^{(2)}$	$t_{2g}^{(3)}$	$e_g^{(1)}$	$e_g^{(2)}$	$t_{2g}^{(1)}$	$t_{2g}^{(2)}$	$t_{2g}^{(3)}$
			$U^s_{i\uparrow j\uparrow}$					$J^s_{i\uparrow j\uparrow}$		
$e_g^{(1)}$	8.4 (7.4)	6.1 (5.2)	6.8 (5.9)	6.8 (5.9)	6.0 (5.1)		1.15 (1.14)	0.70 (0.70)	0.70 (0.70)	1.06(1.04)
$e_g^{(2)}$	6.1 (5.2)	8.4 (7.5)	6.3 (5.4)	6.3 (5.4)	7.0 (6.2)	1.15 (1.14)		0.94 (0.92)	0.94 (0.92)	0.58(0.58)
$t_{2g}^{(1)}$	6.8 (5.9)	6.3 (5.4)	8.1 (7.2)	6.2 (5.3)	6.2 (5.3)	0.70 (0.70)	0.94 (0.92)		0.93 (0.91)	0.93(0.91)
$t_{2g}^{(2)}$	6.8 (5.9)	6.3 (5.4)	6.2 (5.3)	8.1 (7.2)	6.2 (5.3)	0.70 (0.70)	0.94 (0.92)	0.93 (0.91)		0.93(0.91)
$t_{2g}^{(3)}$	6.0 (5.1)	7.0 (6.2)	6.2 (5.3)	6.2 (5.3)	8.1 (7.2)	1.06 (1.04)	0.58 (0.58)	0.93 (0.91)	0.93 (0.91)	
Average			6.7 (5.9)					0.89 (0.87)		
			$U^s_{i\downarrow j\downarrow}$					$J^s_{i\downarrow j\downarrow}$		
$e_g^{(1)}$	7.9 (7.0)	5.8 (4.9)	6.5 (5.7)	6.5 (5.7)	5.8 (5.0)		1.05 (1.05)	0.66 (0.66)	0.66 (0.66)	1.01 (0.99)
$e_g^{(2)}$	5.8 (4.9)	7.9 (7.0)	6.0 (5.2)	6.0 (5.2)	6.8 (5.9)	1.05 (1.05)		0.90 (0.88)	0.90 (0.88)	0.55 (0.55)
$t_{2g}^{(1)}$	6.5 (5.8)	6.0 (5.2)	7.9 (7.1)	6.1 (5.2)	6.1 (5.2)	0.66 (0.66)	0.90 (0.88)		0.90 (0.89)	0.90 (0.89)
$t_{2g}^{(2)}$	6.5 (5.7)	6.0 (5.2)	6.1 (5.2)	7.9 (7.1)	6.1 (5.2)	0.66 (0.66)	0.90 (0.88)	0.90 (0.89)		0.90 (0.89)
$t_{2g}^{(3)}$	5.8 (5.0)	6.8 (5.9)	6.1 (5.2)	6.1 (5.2)	7.9 (7.1)	1.01 (0.99)	0.55 (0.55)	0.90 (0.89)	0.90 (0.89)	
Average			6.5 (5.7)					0.84 (0.83)		
			$U^s_{i\uparrow j\downarrow}$							
$e_g^{(1)}$	8.1 (7.2)	5.9 (5.0)	6.6 (5.8)	6.6 (5.8)	5.9 (5.0)					
$e_g^{(2)}$	5.9 (5.0)	8.1 (7.2)	6.1 (5.3)	6.1 (5.3)	6.9 (6.0)					
$t_{2g}^{(1)}$	6.6 (5.8)	6.1 (5.3)	8.0 (7.1)	6.1 (5.3)	6.1 (5.3)					
$t_{2g}^{(2)}$	6.6 (5.8)	6.1 (5.3)	6.1 (5.3)	8.0 (7.1)	6.1 (5.3)					
$t_{2g}^{(3)}$	5.9 (5.0)	6.9 (6.0)	6.1 (5.3)	6.1 (5.3)	8.0 (7.1)					
Average			6.6 (5.8)							

TABLE V: Comparison between our results and previous work for NiO. All values are in eV.

	U	J
This work (RPA)	5.8	0.85
This work (cRPA)	6.6	0.86
Karlsson *et al.* (cRPA)[a]	6.6	0.9
Anisimov *et al.* (cLDA)[b]	8.0	0.95
Cococcioni *et al.* (cLDA)[c]	4.6	
Pickett *et al.* (cLDA)[d]	5.1	
Jiang *et al.* (cLDA)[e]	5.2	0.9
Floris *et al.* (cLDA)[f]	5.8	
Empirical method[g]	6.2	0.95
Empirical method[h]	6.7	

[a]Reference 30.
[b]Reference 4.
[c]Reference 8.
[d]Reference 31.
[e]Reference 32.
[f]Reference 33.
[g]Reference 34.
[h]Reference 35.

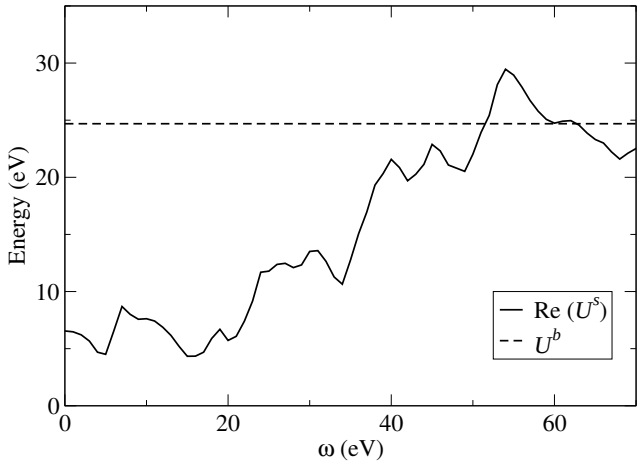

FIG. 7: Frequency-dependence of the screened Coulomb U for d electrons in NiO calculated with the cRPA method. The horizontal dashed line indicates the bare Coulomb energy.

C. $CuGaS_2$

As a last example, and to demonstrate that our method is capable of dealing with more complex materials, we investigate the screened Coulomb interaction for Cu d electrons in $CuGaS_2$. $CuGaS_2$ is a parent material for a large group of Cu-based ternary semiconductors (Cu-III-VI_2, with III = Al, Ga, and In; and VI = S, Se, and Te). These ternary compounds and their solid solutions are among the most promising materials for thin film solar cell absorbers due to their high efficiency and low cost. However, attempts to understand some of the most basic structural and electronic properties of these materials have been complicated by the presence of Cu $3d$ electrons. On one hand, these d electrons are rather localized and experience strong on-site Coulomb correlations. On the other hand, they are relatively shallow in energy and can hybridize with other valence (sp) electrons to form strong covalent bonds. An accurate account of both these aspects of Cu d electrons requires theoretical treatments beyond the conventional DFT method within the LDA or GGA. In a recent paper,[36] we demonstrated that a combined GGA+U and GW approach can reproduce the systematic variation of quasiparticle band gap of Cu-based ternary compounds with chemical constituents. The on-site Coulomb U for Cu d electrons plays an important role in the calculations. Here we present additional details on the calculation of the U and J parameters for $CuGaS_2$.

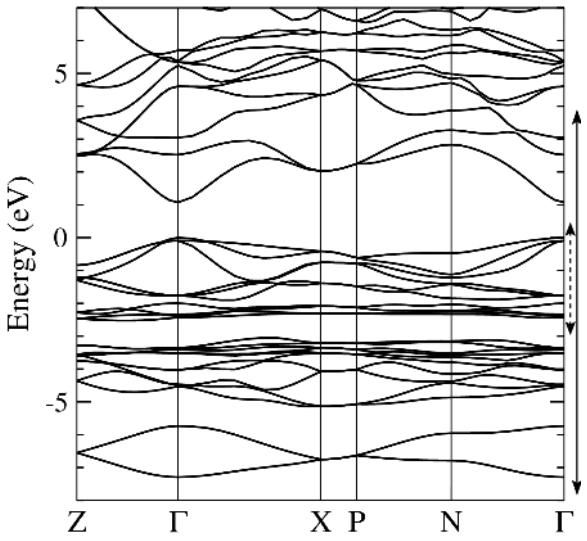

FIG. 8: The GGA+U band structure of $CuGaS_2$. The inner and outer energy windows used for generating MLWF are indicated by the dashed and solid double arrows.

Figure 8 shows the band structure of $CuGaS_2$ calculated using the GGA+U method. To be consistent with our previous work, we use the Perdew-Burke-Ernzerhof GGA functional[37] for this system. The electronic structures of Cu based multinary compounds have been investigated by several groups,[36,38–41] so we will not elaborate on the details of the band structure. Because of

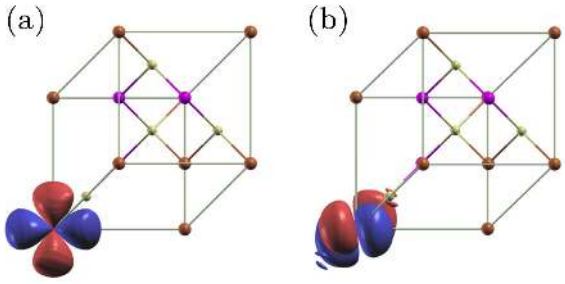

FIG. 9: (Color online) Two representative Cu $3d$-like MLWF in $CuGaS_2$, (a) with the e symmetry and (b) with the t_2 symmetry.

TABLE VI: Screened (bare) Coulomb U and J matrices for Cu $3d$ electrons in $CuGaS_2$ calculated within the cRPA. All values are in eV.

	$U^s_{ij}(U^b_{ij})$					$J^s_{ij}(J^b_{ij})$				
	$e^{(1)}$	$e^{(2)}$	$t_2^{(1)}$	$t_2^{(2)}$	$t_2^{(3)}$	$e^{(1)}$	$e^{(2)}$	$t_2^{(1)}$	$t_2^{(2)}$	$t_2^{(3)}$
$e^{(1)}$	6.2 (25.6)	4.2 (23.3)	4.9 (24.1)	4.9 (24.1)	4.2 (23.2)		1.00 (1.12)	0.64 (0.67)	0.64 (0.67)	1.00 (1.11)
$e^{(2)}$	4.2 (23.3)	6.2 (25.5)	4.4 (23.5)	4.4 (23.5)	5.1 (24.4)	1.00 (1.12)		0.88 (0.97)	0.88 (0.97)	0.52 (0.52)
$t_2^{(1)}$	4.9 (24.1)	4.4 (23.5)	6.1 (25.2)	4.4 (23.3)	4.4 (23.3)	0.64 (0.67)	0.88 (0.97)		0.87 (0.96)	0.88 (0.97)
$t_2^{(2)}$	4.9 (24.1)	4.4 (23.5)	4.4 (23.3)	6.1 (25.2)	4.4 (23.3)	0.64 (0.67)	0.88 (0.97)	0.87 (0.96)		0.88 (0.97)
$t_2^{(3)}$	4.2 (23.2)	5.1 (24.4)	4.4 (23.3)	4.4 (23.3)	6.1 (25.2)	1.00 (1.11)	0.52 (0.52)	0.88 (0.97)	0.88 (0.97)	
Average			4.9 (23.9)					0.82 (0.89)		

the strong *spd* hybridization, the construction of *d*-like MLWF in $CuGaS_2$ requires a more delicate treatment than those in previous cases. We include all S $3p$, Ga $4s$ and Cu $3d$ states in the optimization of the MLWF. The outer and inner energy windows used for the wannierization procedure are shown in Fig. 8. Figure 9 shows two representative MLWF (one with the e symmetry and the other with the t_2 symmetry) on a Cu site, indicating that *d*-like MLWF can be constructed despite a strong entanglement of the d bands with other valence *sp* bands.

Table VI shows the calculated screened and bare onsite U and J matrices for Cu $3d$ electrons in $CuGaS_2$. Due to a strong *spd* hybridization, the $3d$-like MLWF in $CuGaS_2$ are slightly more delocalized than those in ZnO and NiO. Therefore, although the atomic Cu $3d$ electrons have a slightly larger Coulomb integral than Ni $3d$ electrons, the average bare Coulomb U for Cu $3d$-like MLWF in $CuGaS_2$ is only 23.9 eV, which is about 0.9 eV smaller than that for NiO. In addition, the screening effects in this system are substantially stronger than those in NiO since $CuGaS_2$ has a much smaller band gap. As a result, the average screened Coulomb U is only 4.9 eV, which is substantially smaller than that of Ni $3d$ electrons in NiO. Similar to the case of *zb*-ZnO, the e states are slightly more localized than the t_2 states, thus they have a slightly larger screened (or bare) Coulomb U. This is because that the e states, in contrast to the t_2 states which form covalent bonds with valence *sp* states, are nonbonding states and they do not hybridize strongly with valence p states.

V. SUMMARY

In summary, we have developed a combined MLWF and cRPA approach to calculate the screened Coulomb U and exchange J parameters for localized electrons in solid. Our implementation is based on the pseudopotential plane wave and makes use of well developed existing packages, including PARATEC,[20] BerkeleyGW,[22] and WANNIER90.[17] Our approach is capable of calculating (1) the full direct Coulomb and exchange matrices, (2) both the screened and the bare interactions, (3) energy-dependent screening effects, and (4) spin-dependent U and J parameters.

Using this new implementation, we investigate the Coulomb interaction of $3d$ electrons in ZnO, NiO, and $CuGaS_2$. For ZnO, the calculated values of the U and J parameters show little difference between *zb*- and *wz*-phases. However, we find that it is important to calculate these parameters self-consistently. This is true for all systems in which the LDA (or GGA) is not able to provide a reasonable description for the ground state properties. Our results for NiO ($U = 6.6$ eV, $J = 0.86$ eV) fall within previously used/calculated values ($U = 4.6 - 8.0$ eV) and agree well with recent results of Karlsson *et al.* The strong screening in $CuGaS_2$, in combination with a strong *spd* hybridization, substantially reduces the onsite Coulomb U in this system. Finally, we find that the screening effects on the exchange J are less effective than those on the direct Coulomb U.

Acknowledgments

We thank Takashi Miyake for helpful discussions. We acknowledge the computational support provided by the Center for Computational Research at the University at Buffalo, SUNY. This work is supported by the National Science Foundation under Grant No. DMR-0946404 and by the Department of Energy under Grant No. DE-SC0002623. W. Z. is supported by National Basic Research Program (973-program) of China under Project No. 2007CB607503 and NSFC Grants (50825205, 50821004).

[1] P. Hohenberg and W. Kohn, Phys. Rev. **136**, B864 (1964).
[2] W. Kohn and L. J. Sham, Phys. Rev. **140**, A1133 (1965).
[3] J. P. Perdew and Y. Wang, Phys. Rev. B **33**, 8800 (1986).
[4] V. I. Anisimov, J. Zaanen, and O. K. Andersen, Phys. Rev. B **44**, 943 (1991).
[5] A. I. Liechtenstein, V. I. Anisimov, and J. Zaanen, Phys.

Rev. B **52**, R5467 (1995).
[6] O. Gunnarsson, O. K. Andersen, O. Jepsen, and J. Zaanen, Phys. Rev. B **39**, 1708 (1989).
[7] V. I. Anisimov and O. Gunnarsson, Phys. Rev. B **43**, 7570 (1991).
[8] M. Cococcioni and S. de Gironcoli, Phys. Rev. B **71**, 035105 (2005).
[9] M. Springer and F. Aryasetiawan, Phys. Rev. B **57**, 4364 (1998).
[10] T. Kotani, J. Phys.: Condens. Matter **12**, 2413 (2000).
[11] F. Aryasetiawan, M. Imada, A. Georges, G. Kotliar, S. Biermann, and A. I. Lichtenstein, Phys. Rev. B **70**, 195104 (2004).
[12] F. Aryasetiawan, K. Karlsson, O. Jepsen, and U. Schonberger, Phys. Rev. B **74**, 125106 (2006).
[13] T. Miyake, F. Aryasetiawan, and M. Imada, Phys. Rev. B **80**, 155134 (2009).
[14] O. K. Andersen, Phys. Rev. B **12**, 3060 (1975).
[15] N. Marzari and D. Vanderbilt, Phys. Rev. B **56**, 12847 (1997).
[16] I. Souza, N. Marzari, and D. Vanderbilt, Phys. Rev. B **65**, 035109 (2001).
[17] A. A. Mostofi, J. R. Yates, Y.-S. Lee, I. Souza, D. Vanderbilt, and N. Marzari, Comput. Phys. Commun. **178**, 685 (2008).
[18] M. S. Hybertsen and S. G. Louie, Phys. Rev. B **34**, 5390 (1986).
[19] E. Şaşıoğlu, C. Friedrich, and S. Blügel, Phys. Rev. B **83**, 121101 (2011).
[20] [http://www.nersc.gov/projects/paratec]
[21] P. Zhang, W. Luo, V. H. Crespi, M. L. Cohen, and S. G. Louie, Phys. Rev. B **70**, 085108 (2004).
[22] J. Deslippe, G. Samsonidze, D. Strubbe, M. Jain, M. L. Cohen, and S. G. Louie, e-print arXiv:1111.4429v1.
[23] N. Troullier and J. L. Martins, Phys. Rev. B **43**, 1993 (1991).
[24] H. J. Monkhorst and J. D. Pack, Phys. Rev. B **13**, 5188 (1976).
[25] U. Ozgur, Y. I. Alivov, C. Liu, A. Teke, M. A. Reshchikov, S. Dogan, V. Avrutin, S.-J. Cho, and H. Morkoc, J. Appl. Phys. **98**, 041301 (2005).
[26] C. Liu, F. Yun, and H. Morko, J. Mater. Sci.: Mater Electr. **16**, 555 (2005).
[27] B.-C. Shih, Y. Xue, P. Zhang, M. L. Cohen, and S. G. Louie, Phys. Rev. Lett. **105**, 146401 (2010).
[28] D. van der Marel and G. A. Sawatzky, Phys. Rev. B **37**, 10674 (1988).
[29] T. Miyake and F. Aryasetiawan, Phys. Rev. B **77**, 085122 (2008).
[30] K. Karlsson, F. Aryasetiawan, and O. Jepsen, Phys. Rev. B **81**, 245113 (2010).
[31] W. E. Pickett, S. C. Erwin, and E. C. Ethridge, Phys. Rev. B **58**, 1201 (1998).
[32] H. Jiang, R. I. Gomez-Abal, P. Rinke, and M. Scheffler, Phys. Rev. B **82**, 045108 (2010).
[33] A. Floris, S. de Gironcoli, E. K. U. Gross, and M. Cococcioni, Phys. Rev. B **84**, 161102 (2011).
[34] S. L. Dudarev, L.-M. Peng, S. Y. Savrasov, and J.-M. Zuo, Phys. Rev. B **61**, 2506 (2000).
[35] J. Zaanen and G. A. Sawatzky, J. Solid State Chem. **88**, 8 (1990).
[36] Y. Zhang, X. Yuan, X. Sun, B.-C. Shih, P. Zhang, and W. Zhang, Phys. Rev. B **84**, 075127 (2011).
[37] J. P. Perdew, K. Burke, and M. Ernzerhof, Phys. Rev. Lett. **77**, 3865 (1996).
[38] J. E. Jaffe and A. Zunger, Phys. Rev. B **28**, 5822 (1983).
[39] S. B. Zhang, S.-H. Wei, A. Zunger, and H. Katayama-Yoshida, Phys. Rev. B **57**, 9642 (1998).
[40] S. Chen, X. G. Gong, A. Walsh, and S.-H. Wei, Appl. Phys. Lett. **96**, 021902 (2010).
[41] C. Persson, J. Appl. Phys. **107**, 053710 (2010).